

1 **Estimating the impact of a major hurricane on**
2 **transport processes**

3 Thomas Dobbelaere, Emmanuel Hanert

4 February 15, 2021

5 **Abstract**

6 In most hydrodynamic model studies, currents and waves are simu-
7 lated separately. This is especially true for the simulation of passive
8 drifters, whose trajectories are often computed based solely on cur-
9 rents. Although this simplification holds for most situations, as the
10 force exerted by waves on currents can be neglected in fair weather
11 conditions, it may lead to significant errors in storm conditions, during
12 which local currents are strongly influenced by wind-generated waves.
13 In this study, current-wave interactions in heavy-wind conditions are
14 studied by coupling the unstructured-mesh hydrodynamic model SLIM
15 with the wave model SWAN in the Florida Reef Tract during Hurricane
16 Irma (Sep. 2017). This coupled model successfully reproduced both
17 the observed wave behavior and storm surge during the hurricane.
18 The modeled currents were then used to simulate the trajectories of
19 passive drifters during the passage of the hurricane. Our results show
20 that taking wave force into account induces variations of up 1 m/s in
21 modelled currents on the continental shelf break as well as in the vicin-
22 ity of reefs and islands. Wave-current interactions can therefore deflect
23 the trajectories of drifting material by up to 10 km during heavy-wind
24 events. These results strongly advocate for the inclusion of wave forces
25 while studying transport processes (sediments, pollutants, larvae, etc.)
26 under storm conditions

27 **1 Introduction**

28 Wave-current interactions in coastal areas are of great importance for coastal
29 engineering as they play a key role in sediment transport, morphological
30 evolution and pollutant mixing (Bever and MacWilliams, 2013; Li and Johns,
31 1998). However, these interactions are highly nonlinear and can vary sig-
32 nificantly in space and time (Wu et al., 2011). Wave-induced currents are
33 generated by wave radiation gradients (Longuet-Higgins, 1970), affecting
34 water levels near shorelines and wave breaking points (Longuet-Higgins
35 and Stewart, 1964), while changes in water levels and currents, in turn,
36 affect the motion and evolution of waves (Sikirić et al., 2013). Coupled
37 wave-current models are therefore required to capture these complex inter-
38 actions. As coastal oceans are characterized by local complex geometries
39 with islands, inlets and estuaries, unstructured (usually two-dimensional)
40 models are preferred as structured grid models show limitations in resolving
41 topologically controlled nearshore processes (Wu et al., 2011; Chen et al.,
42 2007). The effect of wave-interactions becomes even more significant in
43 the case of hurricanes, that generate large wind-waves and disturb ocean
44 conditions (Liu et al., 2020) by causing coastal upwellings on continental
45 shelves (Smith, 1982) and inducing strong currents, waves and storm surges
46 in nearshore and coastal regions (Dietrich et al., 2010; Weisberg and Zheng,
47 2006). South Florida and the Gulf of Mexico are particularly vulnerable to
48 hurricanes (Malmstadt et al., 2009) and modelling studies predict tropical
49 cyclones to increase both in frequency and intensity in this region (Mar-
50 sooli et al., 2019; Knutson et al., 2010). Being able to accurately model
51 wave-current interactions in this area becomes thus critical.

52 Individual-based modelling of particulates has been extensively used to
53 study the transport of drifting materials such as pollutants, sediments or
54 larvae (Garcia-Pineda et al., 2020; Liubartseva et al., 2018; Figueiredo et al.,
55 2013; Frys et al., 2020). Although some of these studies take the impact
56 of waves into account by adding Stokes drift velocity, *i.e.* the net drift of a
57 floating particle in the direction of the wave propagation (Van Den Bremer
58 and Breivik, 2018), to the Eulerian currents, they usually neglect the wave-
59 induced currents. Such practice is reasonable in the case of fair weather,
60 when wave-induced forces exerted on currents are relatively smaller, but
61 might lead to significant inaccuracies during storm conditions. To assess

62 the importance of wave-current interactions during a tropical cyclone, we
63 investigated the transport of drifting particulates on the Florida shelf during
64 Hurricane Irma, one of the strongest and costliest tropical cyclones on
65 records in the Atlantic Basin (Chen et al., 2007), that made landfall in Florida
66 in September 2017.

67 In this study, we developed an unstructured coupled wave-current model of
68 South Florida to simulate the ocean circulation during hurricane Irma. Both
69 modelled currents and waves were validated against field measurements
70 and were then used to simulate the transport of drifting particulates in the
71 Florida Keys and the Florida inner shelf during the storm. Model outputs
72 were then compared with uncoupled simulation results in order to assess
73 the impact of wave-induced forces and Stokes drift on the modelled currents
74 and transports.

75 **2 Methods**

76 **2.1 Study area and data**

77 Large-scale ocean circulation around South Florida is dominated by the
78 Florida Current (FC), which originates from the Loop Currents (LC) where it
79 enters the Florida Straits from the Gulf of Mexico, and, downstream, forms
80 the Gulf Stream. The FC is a major western boundary current character-
81 ized by spatial variability and meandering, associated with the presence
82 of cyclonic eddies between the core of the current and the complex reef
83 topography of the Florida Reef Tract (FRT) (Frys et al., 2020; Lee et al.,
84 1995; Kourafalou and Kang, 2012). The northern half of these reefs are
85 made of early Holocene reef frameworks and indurated sand ridges while
86 the southern part (the Florida Keys) is composed of a chain of limestone is-
87 lands, fossilized remnants of ancient coral reefs and sand bars (Hoffmeister
88 and Multer, 1968; Shinn, 1988; Lidz and Shinn, 1991). The variability of the
89 FC extends over a large range of spatial and temporal scales, with periods
90 of 30-70 days in the Lower Keys (Lee et al., 1995) and shorter periods of
91 2-21 days in the Upper Keys (Lee and Mayer, 1977), and exhibits significant
92 seasonal and interannual cycles (Johns and Schott, 1987; Lee and Williams,
93 1988; Schott et al., 1988). Circulation on the West Florida Shelf (WFS) on

94 the other hand is forced by local winds and tidal fluctuations (Lee and Smith,
95 2002; Liu and Weisberg, 2012).

96 Field observations were used to validate our model outputs. Modelled sea
97 surface elevation was validated against tide gauge measurements from
98 the National Oceanic and Atmospheric Administrations (NOAA) Tides and
99 Currents dataset. These measurements were taken at four locations: two
100 in the Florida Keys (Key West and Vaca Key); one on the eastern coast
101 of Florida (Key West); and one on the western coast (Naples). Currents
102 were validated against ADCP measurements from the University of South
103 Florida's College of Marine Science's (USF/CMS) Coastal Ocean Monitoring
104 and Prediction System (COMPS) for the WFS (Weisberg et al., 2009). More
105 specifically, we used measurements from moorings C10, C12 and C13,
106 respectively located at the 25, 50, and 50 m isobaths of the WFS (Liu
107 et al., 2020). Finally, validation of modelled wave parameters was performed
108 against four buoy measurements from NOAA's National Data Buoy Center
109 (NDBC): two on Florida's Eastern shelf and two on the WFS. The locations
110 of all measurement stations are shown on Fig. 1

111 **2.2 Wind and atmospheric pressure for Hurricane Irma**

112 Irma made landfall in Florida on 10 September 2017 as a category 3 storm,
113 first at Cudjoe Key (Florida Keys) and later on Marco Island, south to Naples
114 (see Fig. 1). It then weakened to a category 2 storm as it moved further
115 inland (Pinelli et al., 2018). The storm caused damages to up to 75% of
116 the buildings at his landfall point in the Florida Keys, making it one of the
117 strongest and costliest hurricanes on record in the Atlantic basin (Xian et al.,
118 2018; Zhang et al., 2019). The strongest reported wind speed was 50 m/s
119 on Marco Island while the highest recorded storm surge was 2.3 m, although
120 larger wind speed occurred in the Florida Keys (Pinelli et al., 2018) In order
121 to reproduce the wind profile of Irma in our model, high-resolution H*Wind
122 (Powell et al., 1998) wind fields were used. As these data represent 1-min
123 averaged wind speeds, we multiplied them by a factor 0.93 to obtain 10-min
124 averaged wind speeds (Harper et al., 2010), more consistent with the time
125 step of our model. Furthermore, H*Wind wind profiles did not cover the whole
126 model extent during the hurricane and were thus blended within coarser

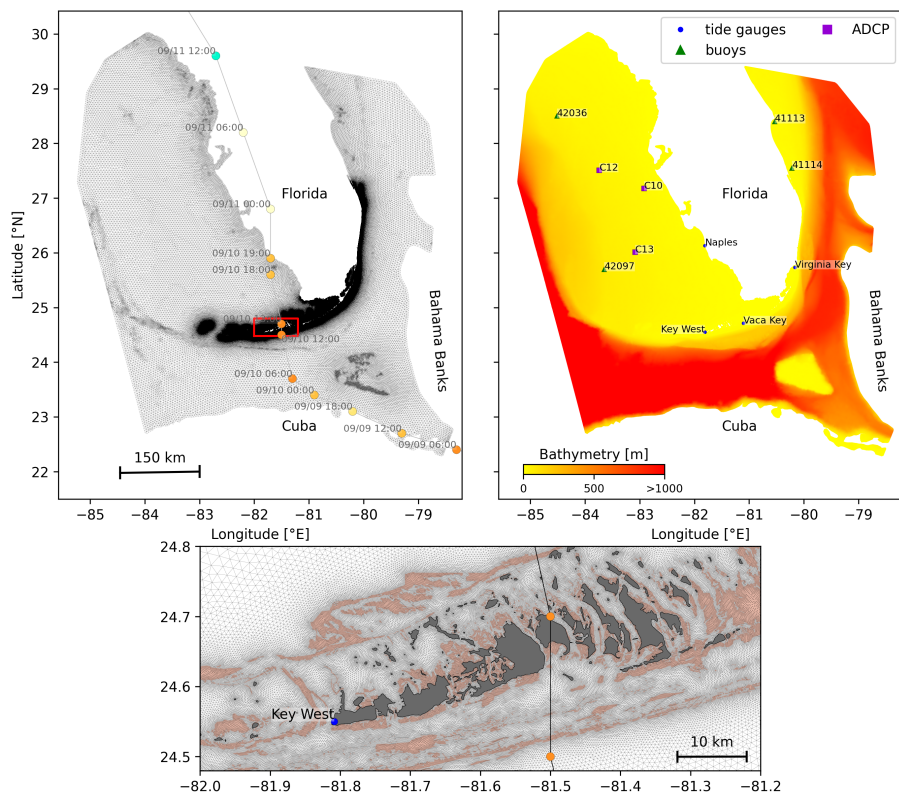


Fig. 1: Upper left: Mesh of the computational domain with the trajectory of Irma, category of the hurricane is given by the Saffir-Simpson color scale. Upper right: Bathymetry of the domain with the location of stations used for the validation of the model outputs. Lower center: Close up view of the 100m mesh resolution near reefs and islands; islands are highlighted in dark grey and coral reefs in coral

127 wind field extracted from ECMWF ERA-5 datasets. Pressure fields of Irma
 128 were also constructed using ERA-5 data. However, the coarse resolution
 129 of the data set caused the depression at the center of the hurricane to get
 130 smoothed out, leading to an underestimation of the pressure gradient in our
 131 model (see eq. 1). To better capture the central depression of Irma, we built
 132 a hybrid pressure field using the position and the minimal pressure of the
 133 core of the hurricane based on its track in the HURDAT 2 database (Landsea
 134 and Franklin, 2013). Based on this information, the hybrid pressure field
 135 was constructed by combining an idealized Holland pressure profile (Lin
 136 and Chavas, 2012) within the radius of maximum wind speed of Irma (Knaff
 137 et al., 2018) with ERA-5 pressure field. The transition between from the
 138 Holland profile to ECMWF data outside the radius of maximum wind speed
 139 data was performed using a smooth step function.

140 **2.3 Hydrodynamic model**

141 Ocean currents generated during hurricane Irma around South Florida
 142 were modelled using the unstructured-mesh depth-integrated coast ocean
 143 model SLIM¹. The model mesh covers an area similar to the model extent
 144 of Dobbelaere et al. (2020b), that includes the FRT but also the Florida
 145 Strait and part of the Gulf of Mexico (Figure 1). However, this area has
 146 been slightly extended northeastward and westward in order to include
 147 the location of buoys for wave outputs validation. Furthermore, in order to
 148 withstand potential cell drying due to storm conditions in this study, we used
 149 the conservative mode of SLIM with wetting-drying, whose equations write:

$$\begin{aligned}
 \frac{\partial H}{\partial t} + \nabla \cdot (\mathbf{U}) &= 0 \\
 \frac{\partial \mathbf{U}}{\partial t} + \nabla \cdot \left(\frac{\mathbf{U}\mathbf{U}}{H} \right) &= -f \mathbf{e}_z \times \mathbf{U} + \alpha g H \nabla(H - h) - \frac{1}{\rho} \nabla p_{\text{atm}} + \frac{1}{\rho} \boldsymbol{\tau}_s \quad (1) \\
 &\quad + \nabla \cdot (\nu \nabla \mathbf{U}) - \frac{C_b}{H^2} |\mathbf{U}| \mathbf{U} + \gamma (\mathbf{U}_* - \mathbf{U})
 \end{aligned}$$

150 where H is the water column height and \mathbf{U} is the depth-averaged transport;
 151 f is the Coriolis coefficient; g is the gravitational acceleration; h is the
 152 bathymetry; α is a coefficient stating whether the mesh element is wet

¹<https://www.slim-ocean.be>

153 ($\alpha = 1$) or dry ($\alpha = 0$); ν is the viscosity; C_b is the bottom drag coefficient;
 154 ∇p_{atm} is the atmospheric pressure gradient; τ_s is the surface stress due
 155 to wind; and γ is a relaxation coefficient towards a reference transport \mathbf{U}_* .
 156 As in Frys et al. (2020) and Dobbelaere et al. (2020b), SLIM currents were
 157 relaxed towards HYCOM (Chassignet et al., 2007) in regions where the water
 158 depth exceeds a given threshold. At very high wind speeds, the white cap is
 159 blown off the crest of the waves, which generates a layer of droplets that acts
 160 as a slip layer for the winds at the ocean-atmosphere interface (Holthuijsen
 161 et al., 2012). This causes a saturation of the wind drag coefficient for strong
 162 winds (Donelan et al., 2004; Powell et al., 2003). To account for the impact
 163 of this saturation on the surface wind stress in our model, we implemented
 164 the wind drag parameterization of Moon et al. (2007).

165 The mesh resolution depended on the distance to coastlines and reefs,
 166 bathymetry and bathymetry gradient in order to satisfy SWAN refinement
 167 criterion $h/A \geq a$, where h is the water depth and A is the element area.
 168 The mesh was generated using the Python library seamsh², based on the
 169 the open-source mesh generator GMSH (Geuzaine and Remacle, 2009) and
 170 is composed of approximately 7.7×10^5 elements. The coarsest elements,
 171 far away from the FRT, had a characteristic length size of about 5 km, as
 172 shown in Fig 1 along with the bathymetry of the model domain.

173 2.4 Wave model

174 Waves were modelled using parallel unstructured SWAN (Booij et al., 1999)
 175 on the same mesh as SLIM. This model solves the action balance equation,
 176 which reads (Mei, 1989):

$$\frac{\partial N}{\partial t} + \nabla_x \cdot [(c_g + \mathbf{u})N] + \frac{\partial}{\partial \theta}[c_\theta N] + \frac{\partial}{\partial \sigma}[c_\sigma N] = \frac{S_{in} + S_{ds} + S_{nl}}{\sigma} \quad (2)$$

177 where $N = E/\sigma$ is the wave action density; θ is the wave propagation direc-
 178 tion; σ is the wave relative frequency; c_g is the wave group velocity, \mathbf{u} is SLIM
 179 depth-averaged current velocity; c_θ and c_σ are the propagation velocities in
 180 spectral space due to refraction and shifting in frequency due to variations
 181 in depth and currents; and S_{in} , S_{ds} , and S_{nl} respectively represent wave

²<https://pypi.org/project/seamsh/>

182 growth by wind, wave decay and nonlinear transfers of wave energy through
 183 interactions between triplets and quadruplets. Spectra were discretized with
 184 48 direction bins and 50 frequency bins logarithmically distributed from 0.3 to
 185 2 Hz. Exponential wind growth was parameterized using the formulation of
 186 Janssen (1991), while dissipations by whitecapping and bottom dissipations
 187 followed the formulations of Komen et al. (1984) and Madsen et al. (1989)
 188 respectively. Coefficients for exponential wind growth and whitecapping
 189 parameterizations were based on the results of Siadatmousavi et al. (2011).
 190 Finally, wave boundary conditions were derived from WAVEWATCH III (Tol-
 191 man et al., 2009) spectral outputs at buoy locations. Depth-averaged Stokes
 192 drift was also computed by SWAN using the following formula:

$$\mathbf{u}_s = \int_0^{2\pi} \int_0^{+\infty} \frac{\sigma^3}{h \tanh(2kh)} E(\sigma, \theta) (\cos \theta, \sin \theta) d\sigma d\theta \quad (3)$$

193 where k is the norm of the wave vector; h is the water depth; and $E(\sigma, \theta)$ is
 194 the wave energy density.

195 2.5 Coupled model

196 The coupling between SLIM and SWAN is illustrated in Figure 2. The two
 197 models are run consecutively at each time step. First, SLIM computes the
 198 sea surface elevation η and depth-averaged current velocity $\mathbf{u} = (u, v)$.
 199 These quantities are transferred to SWAN to update the model water depth
 200 as well as the second term of equation 2 governing wave energy propagation
 201 in the geographic space. Moreover, in order for the two model to have con-
 202 sistent bottom dissipation parameterizations, SLIM bottom drag coefficient is
 203 transformed into a roughness length z_0 following the methodology of Dietrich
 204 et al. (2011). This roughness length is then converted into Madsen's bottom
 205 dissipation term in SWAN. SWAN then produces the wave-induced force on
 206 current τ_{wave} by computing the wave radiation stress gradient. This quantity
 207 is used to update the value of the surface stress τ_s in equation 1, that now
 208 becomes the sum of wind and wave-induced forces $\tau_s = \tau_{\text{wind}} + \tau_{\text{wave}}$.

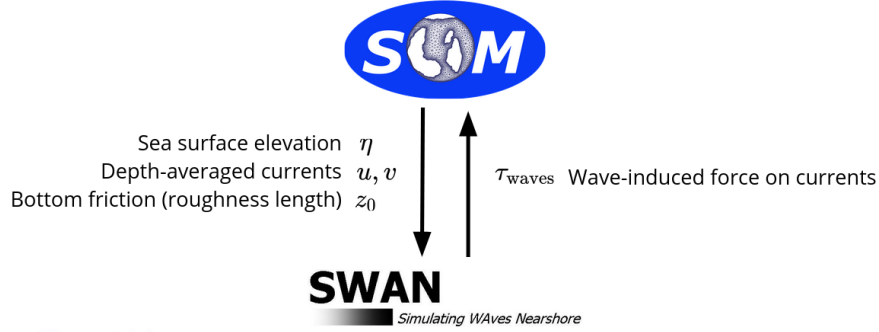


Fig. 2: Schematic illustration of the coupled SLIM+SWAN model.

209 2.6 Comparison of particle trajectories

210 To assess the impact of the wave coupling on the modelled currents during
 211 hurricane Irma, we compared the trajectories of virtual particles driven
 212 by currents produced by SLIM alone and SLIM+SWAN simulations in the
 213 Florida Keys. First, we identified the areas where the differences between
 214 the modelled currents were the largest. Then, we determined the potential
 215 origination regions of particles reaching these areas on the passage of the
 216 hurricane through the Florida Keys using backtracking methods (Dobbelaeere
 217 et al., 2020a). These regions are highlighted by the 4 release regions of Fig.
 218 7. Finally, particles were released from these four regions and advected by
 219 currents produced by the coupled and uncoupled models. At each time step,
 220 the center of mass of the modelled particle clouds were computed. The dis-
 221 tance between these centers of mass was used as a measure of the impact
 222 of the wind-generated wave coupling on the modelled current in the Florida
 223 Keys during hurricane Irma. This comparison was performed with 3 sets
 224 of currents: the currents modelled by uncoupled SLIM (SLIM); the currents
 225 modelled by coupled SLIM+SWAN (SLIM+SWAN); and the SLIM+SWAN
 226 currents with depth-averaged Stokes drift (SLIM+SWAN+Stokes).

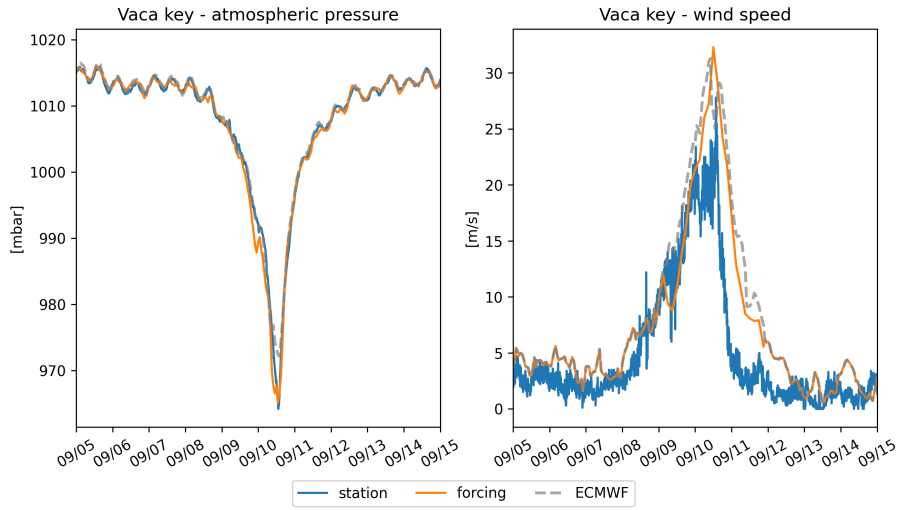


Fig. 3: The atmospheric forcings have been validated with meteorological station observations at Vaca Key. The reconstructed atmospheric pressure and wind speed agree well with field measurements.

227 3 Results

228 3.1 Validation

229 Comparisons of the H*Wind wind and hybrid pressure fields with station
 230 measurements at Vaca Key are shown in Fig. 3. The observed pressure
 231 at the station is well reproduced by the reconstructed hybrid pressure field.
 232 H*Wind profile agree well with field measurements as well despite a slight
 233 overestimation of the peak wind speed.

234 **QUESTION: Should I use quantitative results such as RMSE ?**

235 To validate the hydrodynamic outputs of the coupled wave-current model,
 236 the computed sea surface elevation was compared with tide gauge measure-
 237 ments on the Eastern and Western coasts of Florida as well as in the Florida
 238 Keys. Figure 4 shows a good fit between simulated and measured elevation
 239 at all stations, where the model succeeds in reproducing the observed tide
 240 surge caused by the passage of the Irma. . Measured and modelled depth-
 241 averaged currents at station C10 are shown in Fig. 4. The current speed
 242 and direction during the hurricane agree well with observations.

243 The wave parameters computed by the coupled model were validated

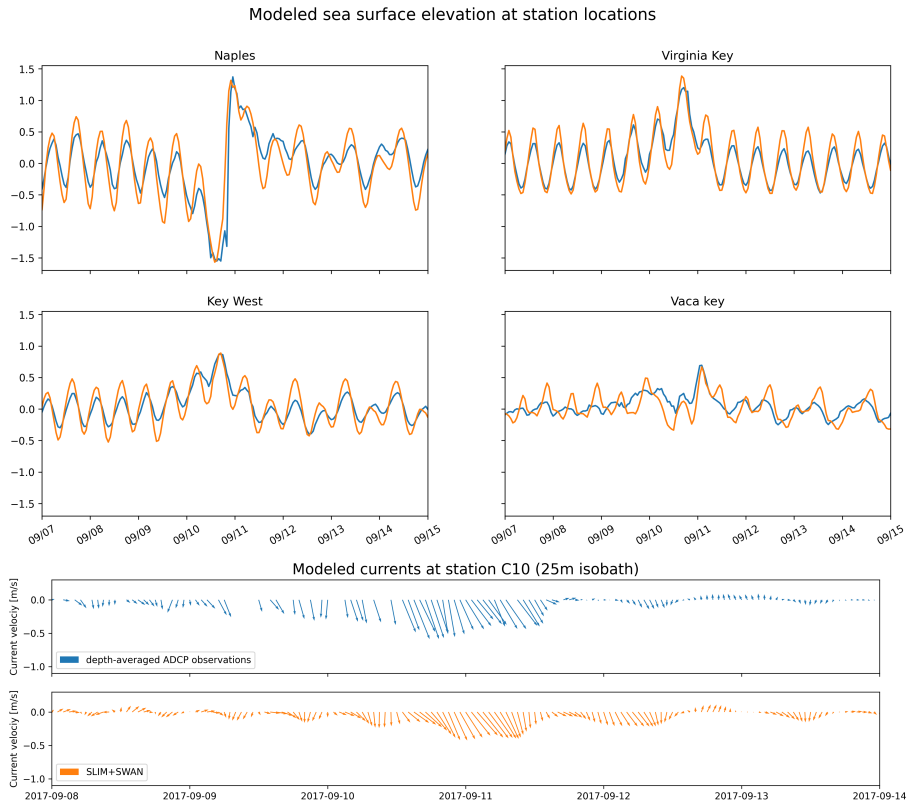


Fig. 4: The sea-surface elevation produced by the coupled wave-current model agrees with SSE and current velocity observations at different stations. The fit is particularly good in the Florida Keys and in Naples, on the inner Florida shelf. The coupled model currents have been validated against current meter data on the inner Florida shelf. The current speed and direction during the hurricane agrees well with the observations.

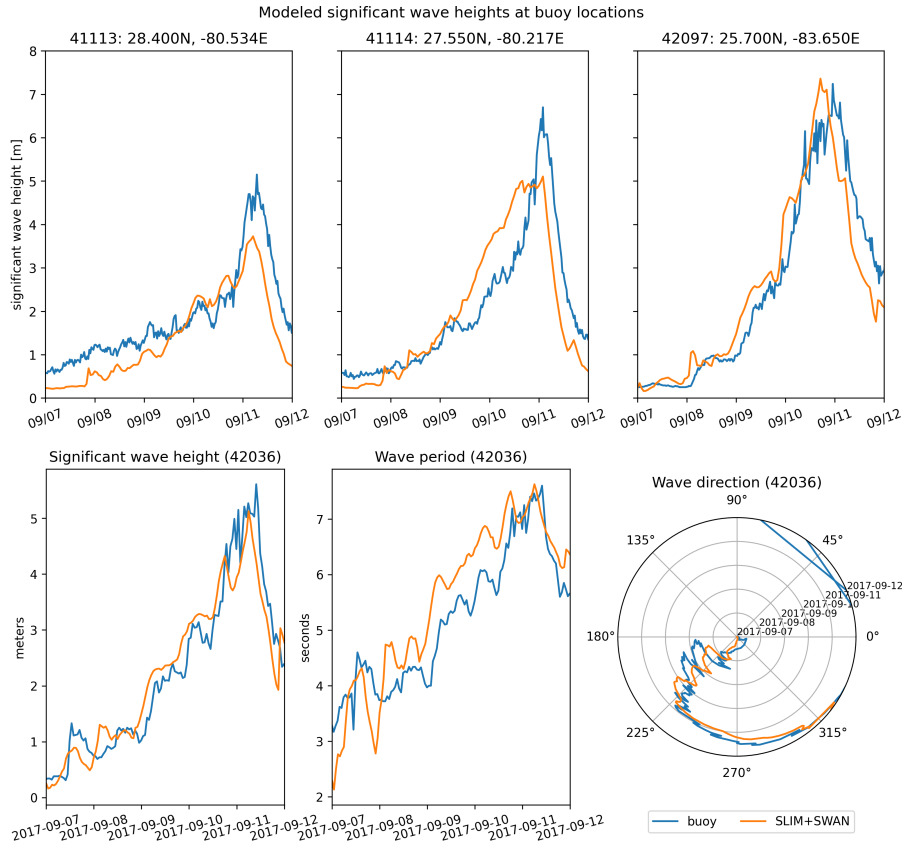


Fig. 5: The significant wave height produced by the coupled model has been compared to buoy measurements at 4 different stations. The timing and amplitude of the peak during the hurricane is correctly reproduced for all stations. For station 42036, the period and direction of the waves also agree well with observations

against field measurements as well. Validation data was extracted from four buoys, two in the Eastern coast Florida and two in the inner shelf. Results of Fig. 5 show that the model reproduces correctly the timing and amplitude of the significant wave height peak during the hurricane for all four stations. Modelled wave period and direction are in good agreement with measurement as well, as shown for station 42036.

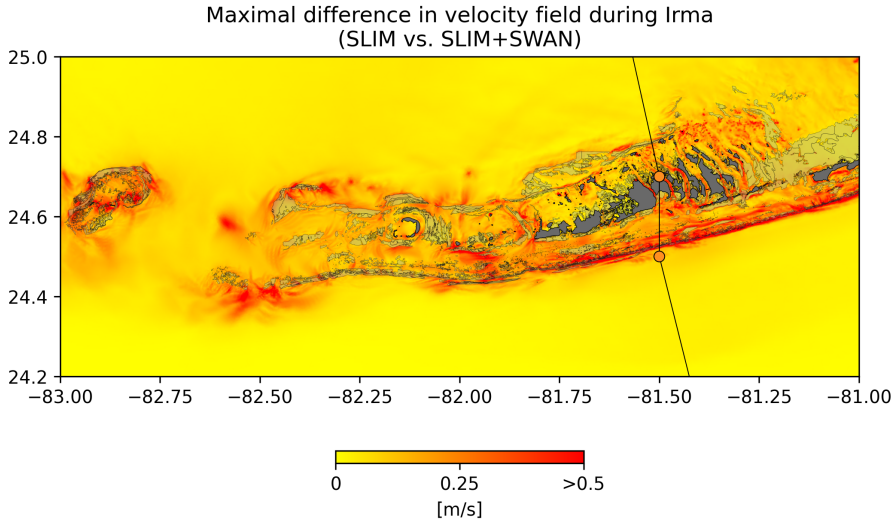


Fig. 6: Maximum of the difference between SLIM and SLIM+SWAN currents speed between 2017-09-07 00:00:00 and 2017-09-13 00:00:00. The difference between the coupled and uncoupled model, which represents the effect of the wave-induced stress, can yield differences of 0.5 m/s in the simulated currents during the passage of the hurricane. SLIM+SWAN currents velocities are larger than the currents modeled by SLIM alone. Islands are highlighted in dark grey and coral reefs in lighter grey

250 3.2 Impact of waves on currents and transport

251 The impact of hurricane-induced wave-current interactions is first evaluated
 252 by computing the norm of the maximal difference in current velocity between
 253 uncoupled SLIM and coupled SLIM+SWAN model runs during the passage
 254 of Irma through the Florida Keys (from 2017-09-07 to 2017-09-13). Figure
 255 6 shows that differences in modelled currents are stronger on the shelf
 256 break and over coral reefs. These results highlight the significant impact
 257 of wave-induced forces, that can yield differences of up to 1 m/s during the
 258 hurricane, with stronger currents being obtained with SLIM+SWAN. This
 259 suggests that neglecting wave-current interactions during Irma would result
 260 in a significant underestimation of transport over reefs.

261 To quantify the impact of these differences in velocity fields on the modelled
 262 trajectories of passive drifters such as coral larvae, we then tracked virtual
 263 particles advected by SLIM, SLIM+SWAN and SLIM+SWAN+Stokes cur-
 264 rents. Comparison of SLIM and SLIM+SWAN+Stokes trajectories are shown

in Fig. 7. Differences between the modelled trajectories are negligible before the passage of the hurricanes in the Florida Keys. Then, distance between the centers of mass of the particles abruptly increase to up to tens of kilometers as Irma gets through the Keys to finally stabilize after the passage of the hurricane. These results support the assumption that wave-induced transport is negligible compared to advection by Eulerian currents in fair weather conditions. However, ignoring waves in storm conditions could result in significant inaccuracies in modelled trajectories, as illustrated in the case of release region 2 in Fig. 7. Particles advected by the currents of the coupled model tend to remain on the shelf while particles advected by SLIM alone are mostly transported along the shelf break. Although not shown in this paper, comparison of SLIM and SLIM+SWAN trajectories were conducted as well. The evolution of the distance between centers of mass of the particle clouds showed similar trends while yielding smaller values. Modelled maximal depth-averaged Stokes drift reached up to 0.2 m/s during the passage of Irma through the Florida Keys. This suggests that both the impact of wave-induced force on Eulerian currents and Stokes drift should be taken into account while modelling particle transport under storm conditions.

4 Discussion and conclusions

- Impact of waves on coral connectivity
- Ability of wave model to correctly capture gradient in significant wave height due to current-waves interactions under tropical cyclones depends on:
 - Spatial (10km → 5km) and spectral (36 dir. → 48 dir.) resolution (Hegermiller et al., 2019)
 - Directional spreading of incident waves (Villas Bôas et al., 2020)

Conflict of Interest Statement

The authors declare that the research was conducted in the absence of any commercial or financial relationships that could be construed as a potential conflict of interest.

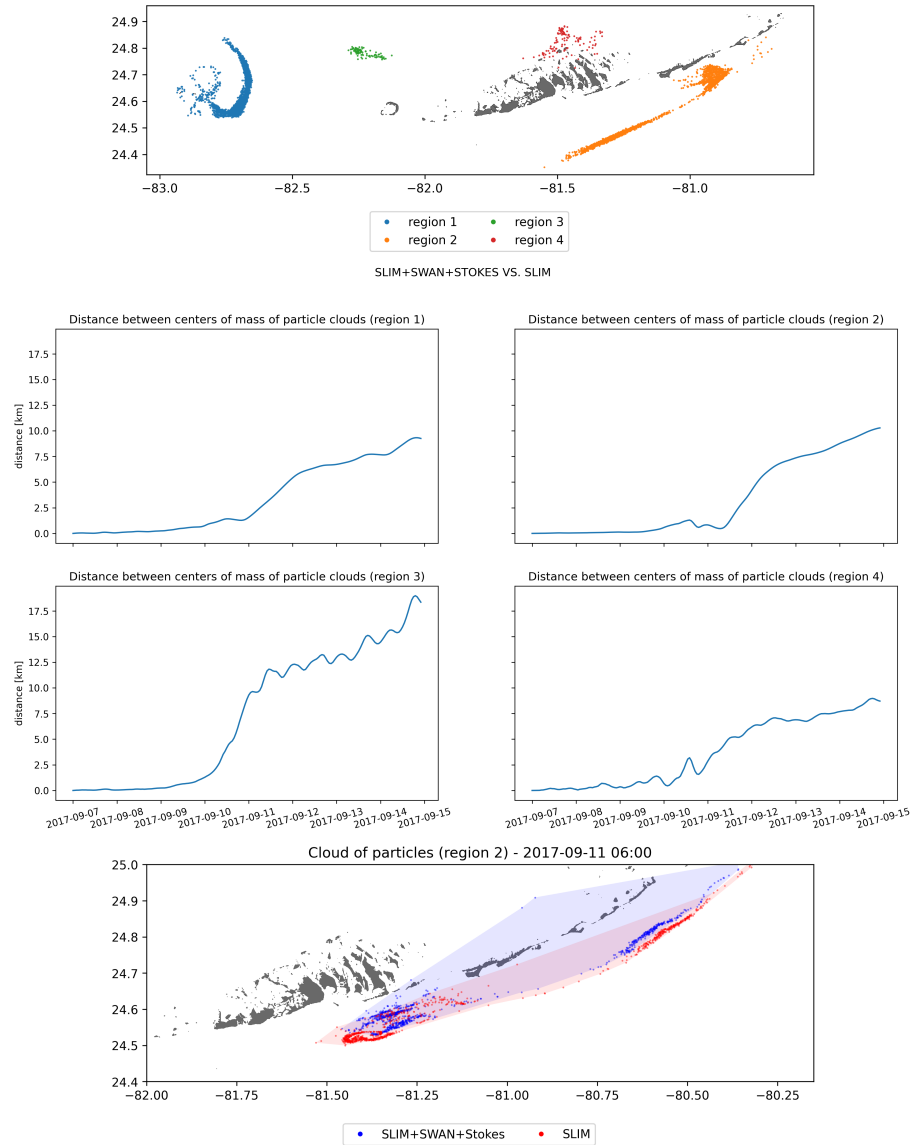


Fig. 7: Comparison of passive drifters trajectories with SLIM+SWAN+Stokes drift vs. SLIM alone. A snapshot of the positions of the particles released from region 2 is shown after the passage of Irma in the Florida Keys. Particles advected by the currents of the coupled model tend to remain on the shelf while particles advected by SLIM alone are mostly transported along the shelf break

²⁹⁴ **Author Contributions**

²⁹⁵ **Funding**

²⁹⁶ **Acknowledgments**

²⁹⁷ Computational resources were provided by the Consortium des Équipements
²⁹⁸ de Calcul Intensif (CÉCI), funded by the F.R.S.-FNRS under Grant No. 2.5020.11.
²⁹⁹ Thomas Dobbelaere is a PhD student supported by the Fund for Research
³⁰⁰ training in Industry and Agriculture (FRIA/FNRS).

³⁰¹ **Supplementary Material**

³⁰² The Supplementary Material for this article is attached to the submitted
³⁰³ document.

³⁰⁴ **References**

- ³⁰⁵ Bever, A. J. and MacWilliams, M. L. (2013). Simulating sediment transport
³⁰⁶ processes in San Pablo Bay using coupled hydrodynamic, wave, and
³⁰⁷ sediment transport models. *Marine Geology*, 345:235–253.
- ³⁰⁸ Booij, N., Ris, R. C., and Holthuijsen, L. H. (1999). A third-generation wave
³⁰⁹ model for coastal regions: 1. Model description and validation. *Journal*
³¹⁰ *of geophysical research: Oceans*, 104(C4):7649–7666.
- ³¹¹ Chassignet, E. P., Hurlbert, H. E., Smedstad, O. M., Halliwell, G. R., Hogan,
³¹² P. J., Wallcraft, A. J., Baraille, R., and Bleck, R. (2007). The HYCOM
³¹³ (hybrid coordinate ocean model) data assimilative system. *Journal of*
³¹⁴ *Marine Systems*, 65(1-4):60–83.
- ³¹⁵ Chen, C., Huang, H., Beardsley, R. C., Liu, H., Xu, Q., and Cowles, G. (2007).
³¹⁶ A finite volume numerical approach for coastal ocean circulation studies:
³¹⁷ Comparisons with finite difference models. *Journal of Geophysical*
³¹⁸ *Research: Oceans*, 112(C3).

- 319 Dietrich, J., Bunya, S., Westerink, J., Ebersole, B., Smith, J., Atkinson,
320 J., Jensen, R., Resio, D., Luettich, R., Dawson, C., et al. (2010). A
321 high-resolution coupled riverine flow, tide, wind, wind wave, and storm
322 surge model for southern Louisiana and Mississippi. part ii: Synoptic
323 description and analysis of hurricanes Katrina and Rita. *Monthly Weather
Review*, 138(2):378–404.
- 325 Dietrich, J., Westerink, J., Kennedy, A., Smith, J., Jensen, R., Zijlema, M.,
326 Holthuijsen, L., Dawson, C., Luettich, R., Powell, M., et al. (2011).
327 Hurricane Gustav (2008) waves and storm surge: Hindcast, synoptic
328 analysis, and validation in southern Louisiana. *Monthly Weather Review*,
329 139(8):2488–2522.
- 330 Dobbelaere, T., Muller, E., Gramer, L., Holstein, D., and Hanert, E. (2020a).
331 Report on the potential origin of the SCTLD in the Florida Reef Tract.
332 Available online at: [https://floridadep.gov/rcp/coral/documents/
333 report-potential-origin-sctld-florida-reef-tract](https://floridadep.gov/rcp/coral/documents/report-potential-origin-sctld-florida-reef-tract).
- 334 Dobbelaere, T., Muller, E. M., Gramer, L. J., Holstein, D. M., and Hanert, E.
335 (2020b). Coupled epidemi-hydrodynamic modeling to understand the
336 spread of a deadly coral disease in Florida. *Frontiers in Marine Science*,
337 7:1016.
- 338 Donelan, M., Haus, B., Reul, N., Plant, W., Stiassnie, M., Gruber, H., Brown,
339 O., and Saltzman, E. (2004). On the limiting aerodynamic roughness of
340 the ocean in very strong winds. *Geophysical Research Letters*, 31(18).
- 341 Figueiredo, J., Baird, A. H., and Connolly, S. R. (2013). Synthesizing larval
342 competence dynamics and reef-scale retention reveals a high potential
343 for self-recruitment in corals. *Ecology*, 94(3):650–659.
- 344 Frys, C., Saint-Amand, A., Le Hénaff, M., Figueiredo, J., Kuba, A., Walker, B.,
345 Lambrechts, J., Vallaeyns, V., Vincent, D., and Hanert, E. (2020). Fine-
346 scale coral connectivity pathways in the Florida Reef Tract: implications
347 for conservation and restoration. *Frontiers in Marine Science*, 7:312.
- 348 Garcia-Pineda, O., Androulidakis, Y., Le Hénaff, M., Kourafalou, V., Hole,
349 L. R., Kang, H., Staples, G., Ramirez, E., and DiPinto, L. (2020). Mea-
350 suring oil residence time with GPS-drifters, satellites, and Unmanned
351 Aerial Systems (UAS). *Marine pollution bulletin*, 150:110644.

- 352 Geuzaine, C. and Remacle, J.-F. (2009). Gmsh: A 3-d finite element mesh
353 generator with built-in pre-and post-processing facilities. *International*
354 *journal for numerical methods in engineering*, 79(11):1309–1331.
- 355 Harper, B., Kepert, J., and Ginger, J. (2010). *Guidelines for converting*
356 *between various wind averaging periods in tropical cyclone conditions*.
357 Citeseer.
- 358 Hegermiller, C. A., Warner, J. C., Olabarrieta, M., and Sherwood, C. R.
359 (2019). Wave–current interaction between Hurricane Matthew wave
360 fields and the Gulf Stream. *Journal of Physical Oceanography*,
361 49(11):2883–2900.
- 362 Hoffmeister, J. and Multer, H. (1968). Geology and origin of the Florida Keys.
363 *Geological Society of America Bulletin*, 79(11):1487–1502.
- 364 Holthuijsen, L. H., Powell, M. D., and Pietrzak, J. D. (2012). Wind and waves
365 in extreme hurricanes. *Journal of Geophysical Research: Oceans*,
366 117(C9).
- 367 Janssen, P. A. (1991). Quasi-linear theory of wind-wave generation applied
368 to wave forecasting. *Journal of physical oceanography*, 21(11):1631–
369 1642.
- 370 Johns, W. E. and Schott, F. (1987). Meandering and transport variations
371 of the Florida Current. *Journal of physical oceanography*, 17(8):1128–
372 1147.
- 373 Knaff, J. A., Sampson, C. R., and Musgrave, K. D. (2018). Statistical tropi-
374 cal cyclone wind radii prediction using climatology and persistence:
375 Updates for the western North Pacific. *Weather and Forecasting*,
376 33(4):1093–1098.
- 377 Knutson, T. R., McBride, J. L., Chan, J., Emanuel, K., Holland, G., Landsea,
378 C., Held, I., Kossin, J. P., Srivastava, A., and Sugi, M. (2010). Tropical
379 cyclones and climate change. *Nature geoscience*, 3(3):157–163.
- 380 Komen, G., Hasselmann, S., and Hasselmann, K. (1984). On the exis-
381 tence of a fully developed wind-sea spectrum. *Journal of physical*
382 *oceanography*, 14(8):1271–1285.

- 383 Kourafalou, V. H. and Kang, H. (2012). Florida Current meandering and
384 evolution of cyclonic eddies along the Florida Keys Reef Tract: Are they
385 interconnected? *Journal of Geophysical Research: Oceans*, 117(C5).
- 386 Landsea, C. W. and Franklin, J. L. (2013). Atlantic hurricane database un-
387 certainty and presentation of a new database format. *Monthly Weather
388 Review*, 141(10):3576–3592.
- 389 Lee, T. N., Leaman, K., Williams, E., Berger, T., and Atkinson, L. (1995).
390 Florida Current meanders and gyre formation in the southern Straits
391 of Florida. *Journal of Geophysical Research: Oceans*, 100(C5):8607–
392 8620.
- 393 Lee, T. N. and Mayer, D. A. (1977). Low-frequency current variability and
394 spin-off eddies along the shelf off southeast Florida. *Collected Reprints*,
395 1(1):344.
- 396 Lee, T. N. and Smith, N. (2002). Volume transport variability through the
397 Florida Keys tidal channels. *Continental Shelf Research*, 22(9):1361–
398 1377.
- 399 Lee, T. N. and Williams, E. (1988). Wind-forced transport fluctuations of the
400 Florida Current. *Journal of Physical Oceanography*, 18(7):937–946.
- 401 Li, Z. and Johns, B. (1998). A three-dimensional numerical model of surface
402 waves in the surf zone and longshore current generation over a plane
403 beach. *Estuarine, Coastal and Shelf Science*, 47(4):395–413.
- 404 Lidz, B. H. and Shinn, E. A. (1991). Paleoshorelines, reefs, and a rising sea:
405 South florida, usa. *Journal of Coastal Research*, pages 203–229.
- 406 Lin, N. and Chavas, D. (2012). On hurricane parametric wind and appli-
407 cations in storm surge modeling. *Journal of Geophysical Research:
408 Atmospheres*, 117(D9).
- 409 Liu, Y. and Weisberg, R. H. (2012). Seasonal variability on the West Florida
410 shelf. *Progress in Oceanography*, 104:80–98.
- 411 Liu, Y., Weisberg, R. H., and Zheng, L. (2020). Impacts of hurricane Irma
412 on the circulation and transport in Florida Bay and the Charlotte Harbor
413 estuary. *Estuaries and Coasts*, 43(5):1194–1216.

- 414 Liubartseva, S., Coppini, G., Lecci, R., and Clementi, E. (2018). Tracking
415 plastics in the Mediterranean: 2D Lagrangian model. *Marine pollution*
416 *bulletin*, 129(1):151–162.
- 417 Longuet-Higgins, M. S. (1970). Longshore currents generated by obliquely
418 incident sea waves. *Journal of geophysical research*, 75(33):6778–
419 6789.
- 420 Longuet-Higgins, M. S. and Stewart, R. (1964). Radiation stresses in water
421 waves; a physical discussion, with applications. In *Deep sea research and oceanographic abstracts*, volume 11, pages 529–562. Elsevier.
- 423 Madsen, O. S., Poon, Y.-K., and Gruber, H. C. (1989). Spectral wave
424 attenuation by bottom friction: Theory. In *Coastal Engineering 1988*,
425 pages 492–504.
- 426 Malmstadt, J., Scheitlin, K., and Elsner, J. (2009). Florida hurricanes and
427 damage costs. *southeastern geographer*, 49(2):108–131.
- 428 Marsooli, R., Lin, N., Emanuel, K., and Feng, K. (2019). Climate change
429 exacerbates hurricane flood hazards along US Atlantic and Gulf Coasts
430 in spatially varying patterns. *Nature communications*, 10(1):1–9.
- 431 Mei, C. C. (1989). *The applied dynamics of ocean surface waves*, volume 1.
432 World scientific.
- 433 Moon, I.-J., Ginis, I., Hara, T., and Thomas, B. (2007). A physics-based
434 parameterization of air–sea momentum flux at high wind speeds and
435 its impact on hurricane intensity predictions. *Monthly weather review*,
436 135(8):2869–2878.
- 437 Pinelli, J.-P., Roueche, D., Kijewski-Correa, T., Plaz, F., Prevatt, D., Zisis,
438 I., Elawady, A., Haan, F., Pei, S., Gurley, K., et al. (2018). Overview
439 of damage observed in regional construction during the passage of
440 Hurricane Irma over the State of Florida. In *Forensic Engineering 2018: Forging Forensic Frontiers*, pages 1028–1038. American Society of
441 Civil Engineers Reston, VA.
- 443 Powell, M. D., Houston, S. H., Amat, L. R., and Morisseau-Leroy, N. (1998).
444 The HRD real-time hurricane wind analysis system. *Journal of Wind
445 Engineering and Industrial Aerodynamics*, 77:53–64.

- 446 Powell, M. D., Vickery, P. J., and Reinhold, T. A. (2003). Reduced drag coefficient for high wind speeds in tropical cyclones. *Nature*, 422(6929):279–283.
- 449 Schott, F. A., Lee, T. N., and Zantopp, R. (1988). Variability of structure and
450 transport of the Florida Current in the period range of days to seasonal.
451 *Journal of Physical Oceanography*, 18(9):1209–1230.
- 452 Shinn, E. A. (1988). The geology of the Florida Keys. *Oceanus*, 31(1):46–53.
- 453 Siadatmousavi, S. M., Jose, F., and Stone, G. (2011). Evaluation of two WAM
454 white capping parameterizations using parallel unstructured SWAN
455 with application to the Northern Gulf of Mexico, USA. *Applied Ocean
456 Research*, 33(1):23–30.
- 457 Sikirić, M. D., Roland, A., Janeković, I., Tomazić, I., and Kuzmić, M. (2013).
458 Coupling of the Regional Ocean Modeling System (roms) and Wind
459 Wave Model. *Ocean Modelling*, 72:59–73.
- 460 Smith, N. P. (1982). Response of Florida Atlantic shelf waters to hurricane
461 David. *Journal of Geophysical Research: Oceans*, 87(C3):2007–2016.
- 462 Tolman, H. L. et al. (2009). User manual and system documentation of
463 WAVEWATCH III TM version 3.14. *Technical note, MMAB Contribution*,
464 276:220.
- 465 Van Den Bremer, T. and Breivik, Ø. (2018). Stokes drift. *Philosophical Transactions of the Royal Society A: Mathematical, Physical and Engineering Sciences*, 376(2111):20170104.
- 468 Villas Bôas, A. B., Cornuelle, B. D., Mazloff, M. R., Gille, S. T., and Arduin,
469 F. (2020). Wave–current interactions at meso-and submesoscales:
470 Insights from idealized numerical simulations. *Journal of Physical
471 Oceanography*, 50(12):3483–3500.
- 472 Weisberg, R., Liu, Y., and Mayer, D. (2009). Mean circulation on the west
473 Florida continental shelf observed with long-term moorings. *Geophys.
474 Res. Lett.*, 36:L19610.
- 475 Weisberg, R. H. and Zheng, L. (2006). Hurricane storm surge simulations
476 for Tampa Bay. *Estuaries and Coasts*, 29(6):899–913.

- 477 Wu, L., Chen, C., Guo, P., Shi, M., Qi, J., and Ge, J. (2011). A FVCOM-
478 based unstructured grid wave, current, sediment transport model, I.
479 Model description and validation. *Journal of Ocean University of China*,
480 10(1):1–8.
- 481 Xian, S., Feng, K., Lin, N., Marsooli, R., Chavas, D., Chen, J., and Hatzikyri-
482 akou, A. (2018). Brief communication: Rapid assessment of damaged
483 residential buildings in the Florida Keys after Hurricane Irma. *Natural
484 Hazards and Earth System Sciences*, 18(7):2041–2045.
- 485 Zhang, C., Durgan, S. D., and Lagomasino, D. (2019). Modeling risk of man-
486 groves to tropical cyclones: A case study of Hurricane Irma. *Estuarine,
487 Coastal and Shelf Science*, 224:108–116.